RSC Advances

PAPER

View Article Online
View Journal | View Issue



Cite this: *RSC Adv.*, 2021, **11**, 27992

# Enhanced 1.5 μm emission from $Yb^{3+}/Er^{3+}$ codoped tungsten tellurite glasses for broadband near-infrared optical fiber amplifiers and tunable fiber lasers

Jian Yuan, *[ab] Guodong Zheng,[a] Yingyi Ye,[a] Yongbin Chen,[a] Tingting Deng,[a] Peng Xiao,[a] Yichen Ye[b] and Weichao Wang[b]

Strong 1.5 μm emission with full width at half maximum (FWHM) of 64 nm has been obtained in 3 mol% $Yb_2O_3$ and 1 mol% $Er_2O_3$ codoped tungsten tellurite glass under the excitation of a 980 nm laser diode. Spectroscopic properties of $Yb^{3+}/Er^{3+}$ codoped tungsten tellurite glasses as a function of $Yb^{3+}$ and $Er^{3+}$ contents are systematically investigated by absorption spectra, emission spectra and lifetime measurement. The structure of tungsten tellurite glass is characterized by Raman spectrum. In addition, emission cross section and gain coefficient of $Er^{3+}$ ions near 1.5 μm are determined and respective maximum values attain $1.06 \times 10^{-20}$ $cm^2$ and 4.07 $cm^{-1}$. Moreover, gain bandwidth and figure of merit associated with gain properties in tungsten tellurite glass are calculated and compared with other reported glasses. These results indicate that $Yb^{3+}/Er^{3+}$ codoped tungsten tellurite glasses with better gain properties are promising candidates in constructing broadband optical fiber amplifiers and tunable fiber lasers in the optical telecommunication window.

Received 8th July 2021
Accepted 13th August 2021

DOI: 10.1039/d1ra05269a

rsc.li/rsc-advances



## 1. Introduction

In the past few decades, wavelength-division-multiplexing (WDM) technology has been extensively used in optical communication systems to meet the rapid increase in demand for information transmission capacity of networks.[1–3] Optical fiber amplifiers with broadband gain bandwidth and high gain are the key devices for WDM network systems.[4] Since the $Er^{3+}$:$^4I_{13/2}$ → $^4I_{15/2}$ radiative transition emits fluorescence at around 1.5 μm that lies in the third optical telecommunication window and $Er^{3+}$ ions can be excited by high power and low cost 980 nm laser diode (LD), $Er^{3+}$ doped fiber amplifiers (EDFA) were initially developed and have been widely used in WDM network systems.[5] At present, most of the commercial EDFA adopted in WDM network systems are made of silica glass. However, silica glass has relatively narrow emission bandwidth at 1.5 μm (~35 nm) and lower doping concentration of $Er^{3+}$ ions resulting in narrow and low gain profile, which limits data transmission capacity of WDM systems.[2,6]

In order to overcome these shortcomings and achieve broad gain bandwidth and high gain, a lot of works have been dedicated to the exploitation for new glass host materials such as silicate, phosphate, germanate and tellurite glasses.[7–10] Among these glass hosts, tellurite glasses own relatively low phonon energy (650–800 $cm^{-1}$), broad infrared transmission region (up to 5 μm), high rare-earth solubility and refractive index (~2).[11] It is very attractive that tellurite glasses possess a variety of structural units such as $TeO_4$ trigonal bipyramid, $TeO_{3+\delta}$ polyhedron and $TeO_3$ trigonal pyramid, which creates a range of electro-static fields around rare earth ions and thus results in inhomogeneous broadening of the spectrum.[12] Broad gain amplification of more than 20 dB in the wavelength range from 1530 to 1610 nm has been demonstrated in EDFA based on tellurite glass.[10] In addition, $WO_3$ not only improves the thermal stability of tellurite glasses but also creates new structural units such as $WO_4$ tetrahedra and $WO_6$ octahedra.[13–15] Therefore, further inhomogeneous broadening can be expected in tungsten tellurite glasses. On the other hand, co-doping $Yb^{3+}$ ions play a role of sensitization for $Er^{3+}$ ions because $Yb^{3+}$ ions with larger absorption cross section at 980 nm than $Er^{3+}$ ions can enhance the pump efficiency of 980 nm LD and then transfer the energy to $Er^{3+}$:$^4I_{11/2}$ energy level *via* resonant energy transfer process ($Yb^{3+}$:$^2F_{5/2}$ + $Er^{3+}$:$^4I_{15/2}$ → $Yb^{3+}$:$^2F_{7/2}$ + $Er^{3+}$:$^4I_{11/2}$).[5] To further enhance 1.5 μm emission from $Er^{3+}$ through $Yb^{3+}$ → $Er^{3+}$, the optimization of $Yb^{3+}$ and $Er^{3+}$ doping concentrations are very essential.

In the present work, we systematically study spectroscopic properties of $Yb^{3+}/Er^{3+}$ codoped tungsten tellurite glasses as a function of $Yb^{3+}$ and $Er^{3+}$ concentrations by absorption spectra, emission spectra and lifetime measurement. The structure of tungsten tellurite glass is characterized by Raman

[a]*Guangdong-Hong Kong-Macao Joint Laboratory for Intelligent Micro-Nano Optoelectronic Technology, Foshan University, Foshan 528000, China. E-mail: yuanjian054@163.com*

[b]*School of Physics and Optoelectronics, State Key Laboratory of Luminescent Materials and Devices, Guangdong Provincial Key Laboratory of Fiber Laser Materials and Applied Techniques, South China University of Technology, Guangzhou 510641, China*

spectrum. Furthermore, Judd–Ofelt (J–O) intensity parameters, emission cross section and gain coefficient of $Er^{3+}$:$^4I_{13/2} \rightarrow {}^4I_{15/2}$ transition are evaluated based on absorption and emission spectra. Besides, gain bandwidth and figure of merit associated with gain properties in tungsten tellurite glass are calculated and compared with other reported glasses.

## 2. Experimental methods

Tungsten tellurite glasses with different nominal compositions (in mol%) of $60TeO_2$–$30WO_3$–$3ZnO$–$7La_2O_3$, $60TeO_2$–$30WO_3$–$3ZnO$–$(6-x)La_2O_3$–$1Er_2O_3$–$xYb_2O_3$ ($x = 0$, 1, 2, 3 and 4) and $60TeO_2$–$30WO_3$–$3ZnO$–$(4-y)La_2O_3$–$3Yb_2O_3$–$yEr_2O_3$ ($y = 0$, 0.5, 1, 1.5, 2 and 3) which are henceforth labeled as TW, TWEY-$x$ and TWYE-$y$, respectively, were synthesized by standard melt-quenching method. Since La, Er and Yb belong to lanthanide family, $La^{3+}$ is easily replaced by $Er^{3+}$ and $Yb^{3+}$, which is beneficial to the enhancement of doping concentrations of $Er^{3+}$ and $Yb^{3+}$ in the host glass. $La_2O_3$ may act as glass network modifier. In addition, the addition of ZnO can decrease the melting temperature of the host glass and increase the glass formation ability. All high-purity reagents (99.99% minimum) were weighed and mixed thoroughly before batches of 15 g mixtures were melted in alumina crucibles in an electric furnace at ~850 °C for 30 min. These melts were cast into preheated cylindrical graphite molds and annealed at 450 °C for 2 h to relax the internal stresses, followed by slow cooling to room temperature. Finally, the annealed samples were optically polished to the disks with the size of $\Phi$ 15 mm × 1.5 mm for optical measurements.

Glass density ($\rho$) was calculated by Archimedes' principle using distilled water as an immersed liquid. After obtaining glass density, the total population of $Er^{3+}$ or $Yb^{3+}$ ions ($N$) was determined by the equation:

$$N = \frac{\rho x}{M} \times N_A \quad (1)$$

where $N$'s unit is $cm^{-3}$, $x$ stands for the doping concentration of $Er^{3+}$ or $Yb^{3+}$ ions (mol%), $M$ represents the average molecular mass of glass and $N_A$ is Avogadro's number.

The refractive indices at 632.8, 1309 and 1533 nm were obtained by the prism coupling method (Metricon model 2010/M, Metricon Corp., America). Raman spectrum was measured by Raman spectrometer (Renishaw inVia, Gloucestershire, UK) and 532 nm laser as the excitation source. Absorption spectra of samples were recorded by Perkin-Elmer Lambda 900 UV/VIS/NIR double beam spectrophotometer (Waltham, MA, America) in the wavelength range from 400 to 2000 nm. The fluorescence spectra were recorded with a computer-controlled iHR 320 spectrofluorometer (Jobin-Yvon Corp., Horiba Scientific, France) under the excitation of a 980 nm LD. The fluorescence signal was collected by InGaAs detector. In addition, the luminescence decay curves of $Er^{3+}$ were measured by a digital oscilloscope (TDS3012C, Tektronix Inc., America) and a function generator (TFG3051C, Tektronix Inc., America) connected to the iHR 320 spectrofluorometer. All of the measurements were carried out at room temperature.

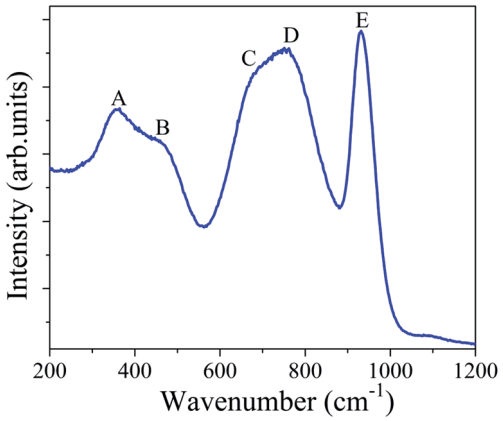


Fig. 1 Raman spectrum of TW glass.

## 3. Results and discussion

### 3.1 Raman and absorption spectra

Fig. 1 represents Raman spectrum of undoped tungsten tellurite glass (TW) in the wavenumber range of 200–1200 $cm^{-1}$. It is observed that five main bands appear in tungsten tellurite glass. The peak A at ~360 $cm^{-1}$ and sharp peak E at ~930 $cm^{-1}$ are attributed to the bending vibrations of corner-shared $WO_6$ octahedra and the vibrations of W–$O^-$ and W=O bonds in $WO_4$ tetrahedra, respectively.[13–15] In addition, the peak B, C and D at ~450, 678 and 750 $cm^{-1}$ are assigned to the symmetrical stretching or bending vibrations of Te–O–Te linkages at corner sharing sites, the anti-symmetric stretching vibrations of Te–O–Te linkages constructed by two un-equivalent Te–O bonds containing bridging oxygens (BO) in $TeO_4$ trigonal bipyramid and the symmetrical stretching vibrations of Te–$O^-$ and Te=O bonds with non-bridging oxygens (NBO) in $TeO_3$ trigonal pyramid and $TeO_{3+1}$ polyhedra, respectively.[15,16] Therefore, very

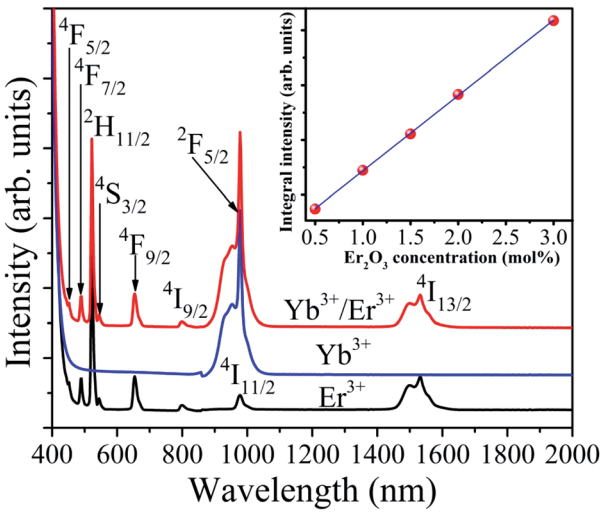


Fig. 2 Absorption spectra of TWEY-0, TWYE-0 and TWYE-1 glasses. The inset shows the integral absorption intensity at 654 nm as a function of $Er_2O_3$ concentration.

Table 1 J–O intensity parameters in $Er^{3+}$ doped TWEY-0 glass and other glass hosts

| Glasses | J–O intensity parameters ($10^{-20}$ cm$^2$) | | | References |
|---|---|---|---|---|
| | $\Omega_2$ | $\Omega_4$ | $\Omega_6$ | |
| Oxyfluoroborosilicate | 6.69 | 3.08 | 3.28 | 22 |
| Phosphate | 3.50 | 0.78 | 0.57 | 23 |
| Fluoride | 3.74 | 1.78 | 1.50 | 24 |
| $TeO_2$–$GeO_2$–$Na_2O$–$Nb_2O_5$ | 6.23 | 1.66 | 1.25 | 25 |
| TWEY-0 | 6.89 | 1.85 | 1.14 | This work |

diverse types of structural units in the present glass can provide various local ligand field environments for $Er^{3+}$ ions in favor of inhomogeneous broadening of 1.5 μm emission band.

Fig. 2 depicts the absorption spectra of $Yb^{3+}$ singly doped, $Er^{3+}$ singly doped and $Yb^{3+}/Er^{3+}$ codoped tungsten tellurite glasses in the wavelength range from 400 to 2000 nm. Different characteristic absorption bands from $Yb^{3+}$ and $Er^{3+}$ ions are labeled in the figure. For $Er^{3+}$ singly doped glass, eight absorption bands are located at 1532, 978, 798, 654, 544, 522, 490 and 452 nm, which are assigned to respective transitions from the $^4I_{15/2}$ ground state to the higher excited states $^4I_{13/2}$, $^4I_{11/2}$, $^4I_{9/2}$, $^4F_{9/2}$, $^4S_{3/2}$, $^2H_{11/2}$, $^4F_{7/2}$ and $^4F_{5/2}$. Energy levels above $^4F_{5/2}$ energy level are not clearly distinguished due to strong intrinsic bandgap absorption in the host glass. It is worth mentioning that absorption bands centered at 978 and 798 nm well match with the laser wavelength of commercial high power 980 and 800 nm LD. Based on the Beer–Lambert equation,[17] absorption cross section at 978 nm ($3.45 \times 10^{-21}$ cm$^2$) is 2.6 times as high as that at 798 nm ($1.32 \times 10^{-21}$ cm$^2$), indicating that more efficient pump absorption can be achieved under the excitation of 980 nm LD. In addition, absorption intensity at 978 nm is greatly enhanced by the addition of $Yb^{3+}$ ions due to $Yb^{3+}$:$^2F_{7/2} \rightarrow {}^2F_{5/2}$ transition. Therefore, $Yb^{3+}/Er^{3+}$ codoped tungsten tellurite glasses can be efficiently pumped by 980 nm LD. The inset of Fig. 2 presents the integral absorption intensity at 654 nm as a function of $Er_2O_3$ concentration. Good linear fitting implies that $Er^{3+}$ ions are uniformly distributed without phase separation and agglomeration in the present tungsten tellurite glasses.[18]

It is well known that J–O theory[19,20] is a common tool to analyze spectroscopic properties of rare-earth (RE) ions doped crystals and glasses. With the help of this theory, three J–O intensity parameters $\Omega_t$ ($t = 2, 4, 6$) of $Er^{3+}$ ions in TWEY-0 glass are determined using Fig. 2 and the procedure introduced elsewhere.[21] Three J–O intensity parameters of $Er^{3+}$ doped TWEY-0 glass are compared with that in other typical glass hosts in Table 1. The root mean square deviation for the best-fitted oscillator strengths is only $2.2 \times 10^{-7}$ for TWEY-0 glass, indicating that calculated J–O intensity parameters are dependable. Higher $\Omega_2$ implies that the degree of asymmetry of coordination environment for RE ions is higher and the covalency between RE ions and ligand is stronger.[21] It is found that $\Omega_2$ of $Er^{3+}$ doped TWEY-0 glass is higher than that of other glass hosts in Table 1, resulted from the co-existence of various structural units as shown in Fig. 1, indicating that Er–O bond in the present glass possesses stronger covalency and coordination environment for $Er^{3+}$ ions is of low symmetry.

### 3.2 Fluorescence spectra, lifetime and energy transfer mechanism

To investigate the effect of $Yb^{3+}$ concentration on spectra properties of TWEY-*x* glasses, near-infrared and upconversion fluorescence spectra are recorded upon 980 nm excitation, as shown in Fig. 3. It is noted from Fig. 3(a) that a strong and broad emission band is located at 1536 nm, attributed to $Er^{3+}$:$^4I_{13/2} \rightarrow {}^4I_{15/2}$ transition. Furthermore, with increasing $Yb_2O_3$ concentration from 0 to 3 mol%, this emission intensity is enhanced by

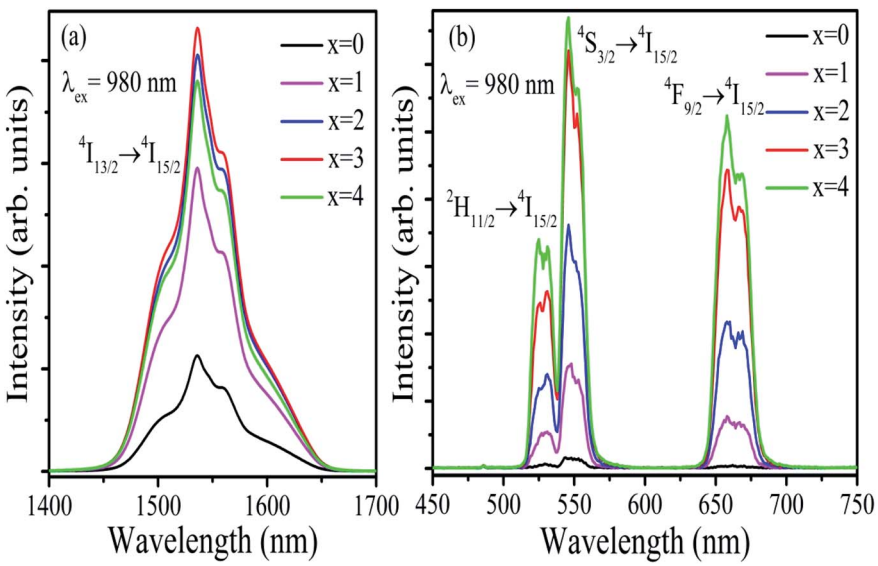


Fig. 3 (a) Near-infrared and (b) upconversion spectra of TWEY-*x* glasses upon 980 nm excitation.

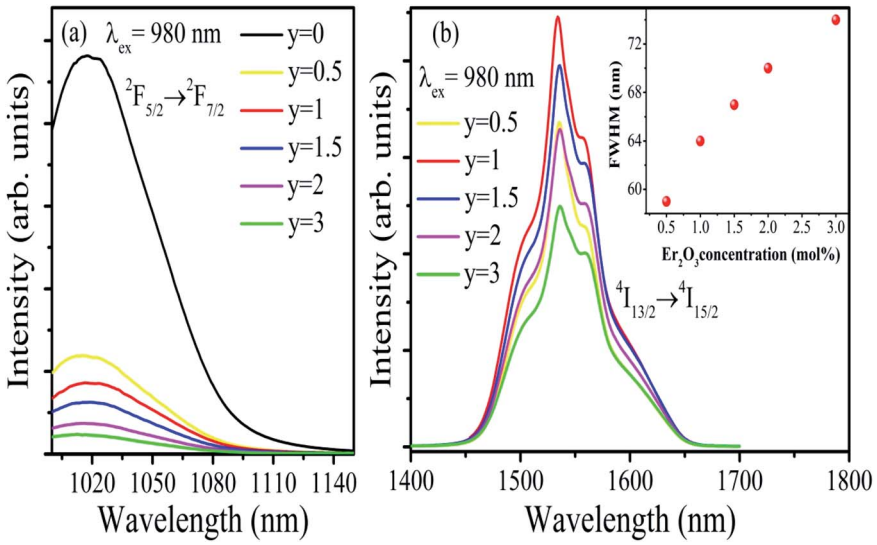


Fig. 4 Near-infrared spectra of TWYE-*y* glasses in the wavelength range of (a) 1000–1150 nm and (b) 1400–1700 nm pumped by 980 nm LD. The inset shows $Er_2O_3$ concentration dependence of FWHM.

about 3 times, which is due to the reduction of the distance between $Yb^{3+}$ and $Er^{3+}$ ions and thus increases the energy transfer probability from $Yb^{3+}$:$^2F_{5/2}$ to $Er^{3+}$:$^4I_{11/2}$ energy level. But the emission intensity begins to reduce with further increasing the concentration, which may be ascribed to concentration quenching phenomenon and the enhancement of upconversion processes, as presented in Fig. 3(b). Three visible fluorescence peaks around 524, 546 and 658 nm appear, corresponding to $Er^{3+}$:$^2H_{11/2} \rightarrow {}^4I_{15/2}$, $^4S_{3/2} \rightarrow {}^4I_{15/2}$ and $^4F_{9/2} \rightarrow {}^4I_{15/2}$ transitions, respectively. Moreover, with the increment of $Yb^{3+}$ content, three visible fluorescence intensities monotonously increase due to the enhancement of energy transfer process from $Yb^{3+}$:$^2F_{5/2}$ to $Er^{3+}$:$^4I_{11/2}$ energy level. Consequently, the optimum concentration of $Yb_2O_3$ is 3 mol% in view of 1.5 μm emission intensity.

In the case where $Yb_2O_3$ concentration is fixed at 3 mol%, near-infrared emission spectra in TWYE-*y* glasses with different $Er_2O_3$ concentration are measured and depicted in Fig. 4 to further discuss energy transfer from $Yb^{3+}$ to $Er^{3+}$ ions. It is found from Fig. 4(a) that with increasing $Er_2O_3$ concentration from 0 to 3 mol%, 1018 nm emission intensity from $Yb^{3+}$:$^2F_{5/2} \rightarrow {}^2F_{7/2}$ transition decreases monotonously, which provides evidence for energy transfer process from $Yb^{3+}$:$^2F_{5/2}$ to $Er^{3+}$:$^4I_{11/2}$ energy level again. It should be mentioned that the emission band centered at 1018 nm can't be completely recorded upon 980 nm excitation because of getting close to the pump wavelength.

The influence of $Er_2O_3$ content on 1.5 μm emission intensity and full width at half maximum (FWHM) is presented in Fig. 4(b). With the argument of $Er_2O_3$ concentration, this intensity heightens gradually due to enhanced energy transfer probability from $Yb^{3+}$ to $Er^{3+}$ before it reaches the maximum value of 1 mol%. And then the intensity decreases gradually with further enhancing the concentration owing to diffusion towards $OH^-$ and other impurities present in the starting materials.[26] The broadening related to 1.5 μm emission band is very important for EDFA, which is usually evaluated by FWHM. Large FWHM is beneficial for wavelength tuning laser and WDM system.[27] The inset of Fig. 4(b) shows that FWHM of $^4I_{13/2} \rightarrow {}^4I_{15/2}$ emission band increases gradually from 59 to 74 nm when $Er_2O_3$ concentration varies from 0.5 to 3 mol%. These values are larger than that in other glass hosts used for optical fiber amplifiers, such as 38 nm in lead borosilicate glasses,[28] 47 nm in lead phosphate glasses,[29] 46 nm in niobium germanate glasses[30] and 48 nm in fluorotellurite glasses.[5] The larger FWHM is ascribed to not only high refractive index (~2.1) which strengthens the ligand fields around $Er^{3+}$ but also to the existence of multiple structural units such as $TeO_4$ trigonal bipyramid, $TeO_3$ trigonal pyramid, $TeO_{3+1}$ polyhedra, $WO_6$ octahedra and $WO_4$ tetrahedra, which creates diverse coordination environments. Therefore, it is in favor of covering the optical communication C (1530–1565 nm) and L (1565–1625 nm) bands and the achievement of tunable fiber lasers.

Fig. 5 shows the fluorescence decay curve of $Er^{3+}$:$^4I_{13/2}$ energy level monitored at 1536 nm in TWYE-1 glass along with the lifetime values in TWYE-*y* glass. It is found that the lifetime of

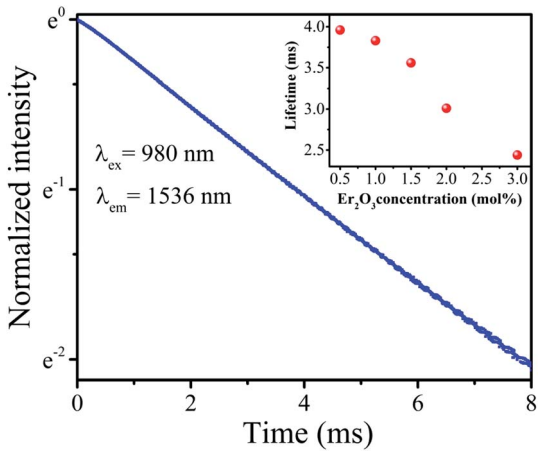


Fig. 5 Fluorescence decay curves of $Er^{3+}$:$^4I_{13/2}$ energy level monitored at 1536 nm in TWYE-1 glass. The inset shows $Er_2O_3$ concentration dependence of the lifetime.

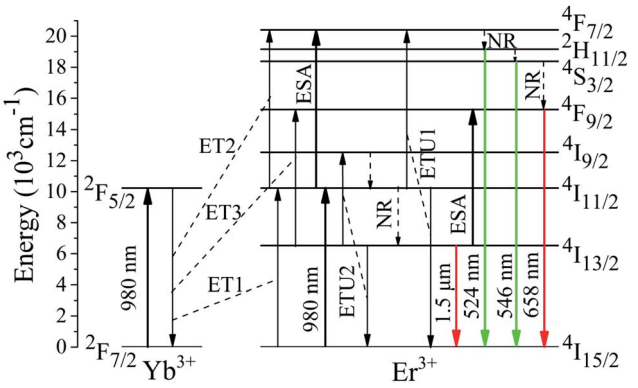


Fig. 6 Simplified energy level diagram and energy transfer mechanism for $Yb^{3+}/Er^{3+}$ codoped tungsten tellurite glasses.

$Er^{3+}$:$^4I_{13/2}$ energy level monotonously reduces from 3.96 to 2.44 ms as $Er_2O_3$ concentration increases from 0.5 to 3 mol%. It is worth noting that the lifetime value slightly changes and is still relatively long (3.83 ms) in TWYE-1 glass.

Based on above-mentioned results, the related energy transfer (ET) mechanism in $Er^{3+}/Yb^{3+}$ codoped tungsten tellurite glasses is illustrated in Fig. 6 with the help of the simplified energy level diagram of $Er^{3+}$ and $Yb^{3+}$. When samples are excited by 980 nm LD, both $Yb^{3+}$ and $Er^{3+}$ ions are initially motivated from the ground states $^2F_{7/2}$ and $^4I_{15/2}$ to the excited states $^2F_{5/2}$ and $^4I_{11/2}$, respectively. Since absorption cross section of $Yb^{3+}$ ions at this wavelength is much larger than that of $Er^{3+}$ ions and $Yb^{3+}$:$^2F_{5/2}$ and $Er^{3+}$:$^4I_{11/2}$ energy levels are closely in resonance, a majority of $Yb^{3+}$ ions transfer their energy to nearby $Er^{3+}$ ions through energy transfer process (ET1): $Yb^{3+}$:$^2F_{5/2}$ + $Er^{3+}$:$^4I_{15/2}$ → $Yb^{3+}$:$^2F_{7/2}$ + $Er^{3+}$:$^4I_{11/2}$, except that a small part of ions de-excite radiatively to $^2F_{7/2}$ energy level and emits fluorescence at 1018 nm. Thereafter, a part of $Er^{3+}$ ions on this energy level relax radiatively and non-radiatively (NR) to $Er^{3+}$:$^4I_{13/2}$ and then return radiatively to the ground state producing fluorescence at 1.5 μm while the remainder is excited to $^4F_{7/2}$ energy level *via* excited state absorption (ESA), ET2: $Yb^{3+}$:$^2F_{5/2}$ + $Er^{3+}$:$^4I_{11/2}$ → $Yb^{3+}$:$^2F_{7/2}$ + $Er^{3+}$:$^4F_{7/2}$ and energy transfer upconversion process (ETU1): $Er^{3+}$:$^4I_{11/2}$ + $Er^{3+}$:$^4I_{11/2}$ → $Er^{3+}$:$^4I_{15/2}$ + $Er^{3+}$:$^4F_{7/2}$. Hence, the green emitting energy levels of $^2H_{11/2}$ and $^4S_{3/2}$ can be populated by relaxing NR from the upper $^4F_{7/2}$ energy level, followed by radiative transitions of $^2H_{11/2}$ → $^4I_{15/2}$ and $^4S_{3/2}$ → $^4I_{15/2}$ emitting fluorescence at 524 and 546 nm. On the other hand, the red emitting energy level of $^4F_{9/2}$ can be populated by ESA, ET3: $Yb^{3+}$:$^2F_{5/2}$ + $Er^{3+}$:$^4I_{13/2}$ → $Yb^{3+}$:$^2F_{7/2}$ + $Er^{3+}$:$^4F_{9/2}$ and relaxing NR from $^2H_{11/2}$ and $^4S_{3/2}$ energy levels. Then radiative transition of $^4F_{9/2}$ → $^4I_{15/2}$ produces fluorescence at 658 nm. It is worth noting that both ESA from $Er^{3+}$:$^4I_{13/2}$ and ETU2: $Er^{3+}$:$^4I_{13/2}$ + $Er^{3+}$:$^4I_{13/2}$ → $Er^{3+}$:$^4I_{15/2}$ + $Er^{3+}$:$^4I_{9/2}$ depopulate $^4I_{13/2}$ energy level and thus lead to decreased emission intensity at 1.5 μm.

### 3.3 Gain properties of $Er^{3+}/Yb^{3+}$ codoped tungsten tellurite glasses

Emission cross section of $Er^{3+}$:$^4I_{13/2}$ → $^4I_{15/2}$ transition is very crucial parameter to evaluate the suitability for broadband EDFA. The emission cross section ($\sigma_e$) can be estimated by the following McCumber formula:[31]

$$\sigma_e(\lambda) = \sigma_a(\lambda)\frac{Z_l}{Z_u}\exp\left(\frac{E_{ZL} - hc/\lambda}{k_B T}\right) \quad (2)$$

where $\sigma_a$ is absorption cross section, $Z_l$ and $Z_u$ represent the partition function of the lower and upper state for $^4I_{13/2}$ → $^4I_{15/2}$ transition, respectively, $k_B$ is the Boltzmann constant, $T$ is the temperature and $E_{ZL}$ is the zero-line energy, defined as the energy difference between the lowest stark of the upper and lower manifolds. The absorption cross section can be estimated by the Beer–Lambert equation:[17]

$$\sigma_a(\lambda) = \frac{2.303\log\left(\frac{I_0}{I}\right)}{Nl} \quad (3)$$

where $I_0$ and $I$ represent the intensities of incident and transmitted light, respectively, $N$ is the total population of $Er^{3+}$ ions and $l$ is the thickness of the sample. According to eqn (1), the total population of $Er^{3+}$ ions in TWYE-1 glass reaches 3.84 × $10^{20}$ cm$^{-3}$ (2 mol%). Fig. 7(a) presents the absorption and emission cross section as a function of wavelength in TWYE-1 glass. It is found that the maximum $\sigma_e$ of $Er^{3+}$ reaches 1.06 × $10^{-20}$ cm$^2$ near 1.5 μm which is larger than those values reported in oxyfluorosilicate glass (4.88 × $10^{-21}$ cm$^2$),[32] lead phosphate glass (4.9 × $10^{-21}$ cm$^2$),[29] bismuthate glass (8.2 × $10^{-21}$ cm$^2$)[33] and gallogermanate glass (7.6 × $10^{-21}$ cm$^2$),[2] indicating that high gain coefficient and low pump threshold can be excepted in the present glass.[34] Large emission cross section of $Er^{3+}$ in TWYE-1 glass is due to high refractive index. The measured refractive indices at 632.8, 1309 and 1533 nm in TWYE-1 glass reach 2.0673, 2.0186 and 2.0152, respectively.

Assuming that $Er^{3+}$ ions are only in either $^4I_{15/2}$ ground state or $^4I_{13/2}$ first excited state, the gain coefficient $G(\lambda)$ near 1.5 μm associated with the absorption and emission cross section is evaluated by the expression to estimate the gain properties qualitatively:[35]

$$G(\lambda) = N[p\sigma_e - (1-p)\sigma_a] \quad (4)$$

where $N$ stands for the total population of $Er^{3+}$ ions and $p$ represents the population inversion defined as the ratio between the population at $^4I_{13/2}$ energy level and the total population. Fig. 7(b) depicts the gain coefficient of $Er^{3+}$:$^4I_{13/2}$ → $^4I_{15/2}$ transition as a function of the wavelength in TWYE-1 glass while $p$ increases from 0 to 1 in step of 0.2. It is noticed that respective wavelength of the maximum gain shifts toward shorter wavelength side as $p$ raises, revealing a typical characteristic of the quasi-three-level system. Moreover, positive gain coefficient is obtained when $p$ is higher than 0.2, indicating a lower pump threshold. It is worth noting that the maximum gain coefficient of TWYE-1 glass is 4.07 cm$^{-1}$ at 1534 nm, which is larger than those values reported in borosilicate glass (1.01 cm$^{-1}$),[22] phosphate glasses (1.02 cm$^{-1}$),[36] bismuthate glass (3.51 cm$^{-1}$)[33] and niobium germanate glass (0.28 cm$^{-1}$).[30]

Gain bandwidth is a key parameter for optical fiber amplifiers and is usually defined as the product of FWHM and

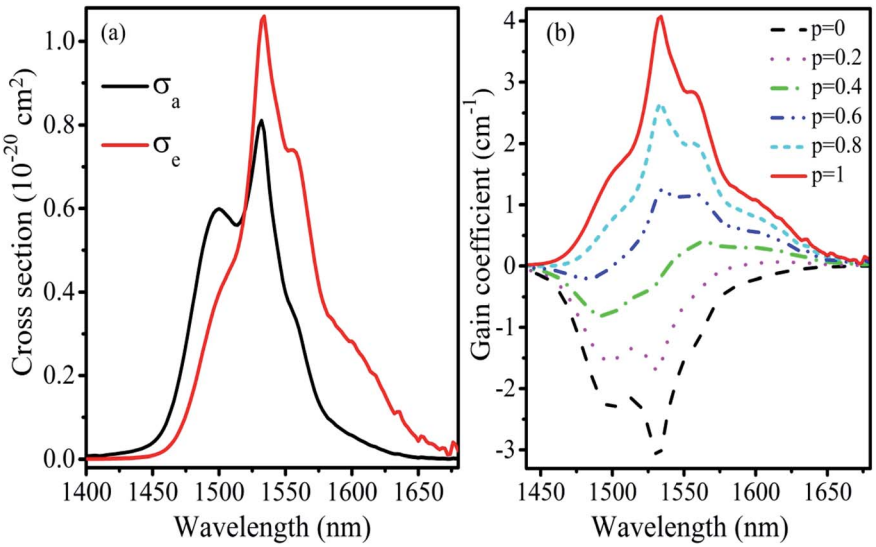


Fig. 7 (a) Absorption and emission cross sections of $Er^{3+}$:$^4I_{13/2} \leftrightarrow {}^4I_{15/2}$ transitions (b) the effect of $^4I_{13/2} \rightarrow {}^4I_{15/2}$ transition wavelength on the gain coefficient in TWYE-1 glass.

emission cross section (FWHM × $\sigma_e$).[37] The larger FWHM × $\sigma_e$ implies the better properties of amplifier. FWHM × $\sigma_e$ in TWYE-1 glass reaches 6.78 × $10^{-26}$ cm,[3] which is larger than those values reported in silicate glass (2.2 × $10^{-26}$ $cm^3$),[38] zinc-fluorophosphate glass (1.61 × $10^{-26}$ $cm^3$),[27] gallogermanate glass (4.02 × $10^{-26}$ $cm^3$)[2] and zinctellurite glass (4.91 × $10^{-26}$ $cm^3$).[37] On the other hand, the figure of merit (FOM) is another vital parameter for optical fiber amplifiers to achieve high gain amplification, which is usually defined as the product of emission cross section and measured lifetime.[39] The larger FOM indicates a lower pump threshold. FOM in TWYE-1 glass reaches 4.06 × $10^{-23}$ $cm^2$ s, which is higher than that in silicate glass (2.09 × $10^{-23}$ $cm^2$ s),[38] zincfluorophosphate glass (1.26 × $10^{-23}$ $cm^2$ s),[27] germanate glass (2.89 × $10^{-23}$ $cm^2$ s)[40] and fluorotellurite glass (1.84 × $10^{-23}$ $cm^2$ s).[38] As a consequence, $Yb^{3+}$/$Er^{3+}$ codoped tungsten tellurite glasses with larger emission cross section and better gain properties are potential candidates for broadband optical fiber amplifiers and tunable fiber lasers.

## 4. Conclusions

In conclusion, $Yb^{3+}$/$Er^{3+}$ codoped tungsten tellurite glasses with a series of doping concentration were prepared and their spectroscopic characteristics dependence of $Yb^{3+}$ and $Er^{3+}$ concentrations under 980 nm excitation were measured and studied in detail. Strong 1.5 μm emission with FWHM of 64 nm has been achieved in tungsten tellurite glass codoped with 3 mol% $Yb_2O_3$ and 1 mol% $Er_2O_3$, profiting from enormous absorption coefficient of $Yb^{3+}$ ions at the pump wavelength and efficient resonance energy transfer process from $Yb^{3+}$:$^2F_{5/2}$ to $Er^{3+}$:$^2I_{11/2}$ energy level. Furthermore, the present glass owns multiple structural units and shows long lifetime of $Er^{3+}$:$^4I_{13/2}$ energy level (3.96 ms), high emission cross section (1.06 × $10^{-20}$ $cm^2$) and gain coefficient (4.07 $cm^{-1}$) near 1.5 μm, resulting in larger gain bandwidth (6.78 × $10^{-26}$ $cm^3$) and figure of merit (4.06 × $10^{-23}$ $cm^2$ s) than those values reported in other glasses. In consequence, these results indicate that $Yb^{3+}$/$Er^{3+}$ codoped tungsten tellurite glasses with better gain properties are promising candidates in constructing broadband optical fiber amplifiers and tunable fiber lasers in the optical telecommunication window.

## Author contributions

Jian Yuan conceived the idea and supervised the experimental work and paper writing. Guodong Zheng and Yingyi Ye performed the sample preparation. Yongbin Chen and Yichen Ye performed the optical measurements. Tingting Deng, Peng Xiao and Weichao Wang contributed to data analysis and secured funding. All authors reviewed the manuscript.

## Conflicts of interest

There are no conflicts to declare.

## Acknowledgements

The authors gratefully acknowledge the financial support from the National Natural Science Foundation of China (Grant No. 51902053, 61804029), Natural Science Foundation of Guangdong Province (Grant No. 2019A1515011988), Guangdong Basic and Applied Basic Research Foundation (Grant No. 2019A1515110002), the Foundation for Distinguished Young Talents in Higher Education of Guangdong (Grant No. 2019KQNCX172), the Project of Foshan Education Bureau (Grant No. 2019XJZZ02), Research Fund of Guangdong-Hong Kong-Macao Joint Laboratory for Intelligent Micro-Nano Optoelectronic Technology (Grant No. 2020B1212030010), the Open Fund of the State Key Laboratory of Luminescent Materials and Devices (South China University of Technology, Grant No. 2020-

skllmd-13) and the Open Fund of the Guangdong Provincial Key Laboratory of Fiber Laser Materials and Applied Techniques (South China University of Technology, Grant No. 2021-07).

## References

1 H. Hu and L. K. Oxenløwe, Chip-based optical frequency combs for high-capacity optical communications, *Nanophotonics*, 2021, **10**(5), 1367–1385.

2 D. M. Shi, Y. G. Zhao, X. F. Wang, G. H. Liao, C. Zhao, M. Y. Peng and Q. Y. Zhang, Effects of alkali ions on thermal stability and spectroscopic properties of $Er^{3+}$-doped gallogermanate glasses, *Phys. B*, 2011, **406**, 628–632.

3 A. Q. L. Quang, V. G. Truong, A. M. Jurdyc, B. Jacquier, J. Zyss and I. Ledoux, Gain properties of an $Er^{3+}$ complex in a poly(methylmethacrylate) matrix for 1540 nm broadband optical amplification, *J. Appl. Phys.*, 2007, **101**(2), 023110.

4 Q. L. Chen, H. Wang, Q. W. Wang and Q. P. Chen, Structural study of the origin of the largest 1.5 μm $Er^{3+}$ luminescence band width in multicomponent silicate glass, *J. Non-Cryst. Solids*, 2014, **404**, 145–150.

5 J. M. Liu, X. Huang, H. Pan, X. Zhang, X. J. Fang, W. X. Li, H. Zhang, A. P. Huang and Z. S. Xiao, Broadband near infrared emission of $Er^{3+}$/$Yb^{3+}$ co-doped fluorotellurite glass, *J. Alloys Compd.*, 2021, **866**, 158568.

6 K. Linganna, M. Rathaiah, N. Vijaya, Ch. Basavapoornima, C. K. Jayasankar, S. Ju, W. T. Han and V. Venkatramu, 1.53 μm luminescence properties of $Er^{3+}$-doped K–Sr–Al phosphate glasses, *Ceram. Int.*, 2015, **41**, 5765–5771.

7 M. P. Hehlen, N. J. Cockroft, T. R. Gosnell and A. J. Bruce, Spectroscopic properties of $Er^{3+}$- and $Yb^{3+}$-doped soda-lime silicate and aluminosilicate glasses, *Phys. Rev. B: Condens. Matter Mater. Phys.*, 1997, **56**(15), 9302–9318.

8 Y. Zhang, M. M. Li, J. Li, J. Tang, W. J. Cao and Z. N. Wu, Optical properties of $Er^{3+}$/$Yb^{3+}$ co-doped phosphate glass system for NIR lasers and fiber amplifiers, *Ceram. Int.*, 2018, **44**, 22467–22472.

9 T. Wei, F. Z. Chen, Y. Tian and S. Q. Xu, 1.53 μm emission properties in $Er^{3+}$ doped $Y_2O_3$ and $Nb_2O_5$ modified germanate glasses for an optical amplifier, *J. Lumin.*, 2014, **154**, 41–45.

10 Y. Ohishi, A. Mori, M. Yamada, H. Ono, Y. Nishida and K. Oikawa, Gain characteristics of tellurite-based erbium-doped fiber amplifiers for 1.5 μm broadband amplification, *Opt. Lett.*, 1998, **23**(4), 274–276.

11 B. Richards, A. Jha, Y. Tsang, D. Binks, J. Lousteau, F. Fusari, A. Lagatsky, C. Brown and W. Sibbett, Tellurite glass lasers operating close to 2 μm, *Laser Phys. Lett.*, 2010, **7**(3), 177–193.

12 A. Jha, S. Shen and M. Naftaly, Structural origin of spectral broadening of 1.5 μm emission in $Er^{3+}$-doped tellurite glasses, *Phys. Rev. B: Condens. Matter Mater. Phys.*, 2000, **62**(10), 6215–6227.

13 B. V. R. Chowdari and P. P. Kumari, Raman spectroscopic study of ternary silver tellurite glasses, *Mater. Res. Bull.*, 1999, **34**(2), 327–342.

14 J. Yuan, Q. Yang, D. D. Chen, Q. Qian, S. X. Shen, Q. Y. Zhang and Z. H. Jiang, Compositional effect of $WO_3$, $MoO_3$, and $P_2O_5$ on Raman spectroscopy of tellurite glass for broadband and high gain Raman amplifier, *J. Appl. Phys.*, 2012, **111**(10), 103511.

15 R. Jose, Y. Arai and Y. Ohishi, Raman scattering characteristics of the TBSN-based tellurite glass system as a new Raman gain medium, *J. Opt. Soc. Am. B*, 2007, **24**(7), 1517–1526.

16 J. Yuan, W. C. Wang, Y. C. Ye, T. T. Deng, D. Q. Ou, J. Y. Cheng, S. J. Yuan and P. Xiao, Effect of $BaF_2$ variation on spectroscopic properties of $Tm^{3+}$ doped gallium tellurite glasses for efficient 2.0 μm laser, *Front. Chem.*, 2021, **8**, 628273.

17 K. F. Li, Q. Zhang, G. X. Bai, S. J. Fan, J. J. Zhang and L. L. Hu, Energy transfer and 1.8 μm emission in $Tm^{3+}$/$Yb^{3+}$ codoped lanthanum tungsten tellurite glasses, *J. Alloys Compd.*, 2010, **504**, 573–578.

18 W. C. Wang, L. Y. Mao, J. L. Liu and S. H. Xu, Glass-forming regions and enhanced 2.7 μm emission by $Er^{3+}$ heavily doping in $TeO_2$–$Ga_2O_3$–$R_2O$ (or MO) glasses, *J. Am. Ceram. Soc.*, 2020, **103**, 4999–5012.

19 B. R. Judd, Optical absorption intensities of rare-earth ions, *Phys. Rev.*, 1962, **127**(3), 750–761.

20 G. S. Ofelt, Intensities of crystal spectra of rare-earth ions, *J. Chem. Phys.*, 1962, **37**(3), 511–520.

21 Y. A. Lakshmi, K. Swapna, K. S. R. K. Reddy, M. Venkateswarlu, Sk. Mahamuda and A. S. Rao, Structural and optical NIR studies of $Er^{3+}$ ions doped bismuth boro tellurite glasses for luminescence materials applications, *J. Lumin.*, 2019, **211**, 39–47.

22 M. Rajesh, M. R. Babu, N. J. Sushma and B. D. P. Raju, Influence of $Er^{3+}$ ions on structural and fluorescence properties of $SiO_2$–$B_2O_3$–$Na_2CO_3$–NaF–$CaF_2$ glasses for broadband 1.53 μm optical amplifier applications, *J. Non-Cryst. Solids*, 2020, **528**, 119732.

23 A. A. Reddy, S. S. Babu and G. V. Prakash, $Er^{3+}$-doped phosphate glasses with improved gain characteristics for broadband optical amplifiers, *Opt. Commun.*, 2012, **285**, 5364–5367.

24 F. F. Huang, Y. Tian, S. Q. Xu and J. J. Zhang, Spectroscopic and energy transfer mechanism of $Er^{3+}$, $Pr^{3+}$-codoped ZBYA glass, *Ceram. Int.*, 2016, **42**, 7924–7928.

25 O. B. Silva, V. A. G. Rivera, Y. Ledemi, Y. Messaddeq and E. Marega Jr, Germanium concentration effects on the visible emission properties of $Er^{3+}$ in tellurite glasses, *J. Lumin.*, 2021, **232**, 117808.

26 H. Gebavi, D. Milanese, R. Balda, S. Chaussedent, M. Ferrari, J. Fernandez and M. Ferraris, Spectroscopy and optical characterization of thulium doped TZN glasses, *J. Phys. D: Appl. Phys.*, 2010, **43**, 135104.

27 V. B. Sreedhar, N. Vijaya, D. Ramachari and C. K. Jayasankar, Luminescence studies on $Er^{3+}$-doped zincfluorophosphate glasses for 1.53 μm laser applications, *J. Mol. Struct.*, 2017, **1130**, 1001–1008.

28 M. R. Babu, N. M. Rao and A. M. Babu, Effect of erbium ion concentration on structural and luminescence properties of lead borosilicate glasses for fiber amplifiers, *Luminescence*, 2018, **33**(1), 71–78.

 

29 Ch. Basavapoornima, T. Maheswari, S. R. Depuru and C. K. Jayasankar, Sensitizing effect of $Yb^{3+}$ ions on photoluminescence properties of $Er^{3+}$ ions in lead phosphate glasses: Optical fiber amplifiers, *Opt. Mater.*, 2018, **86**, 256–269.

30 L. M. Marcondes, C. R. D. Cunha, B. P. D. Sousa, S. Maestri, R. R. Gonçalves, F. C. Cassanjes and G. Y. Poirier, Thermal and spectroscopic properties studies of $Er^{3+}$-doped and $Er^{3+}/Yb^{3+}$-codoped niobium germanate glasses for optical applications, *J. Lumin.*, 2019, **205**, 487–494.

31 D. E. McCumber, Einstein relations connecting broadband emission and absorption spectra, *Phys. Rev.*, 1964, **136**(4A), 954–957.

32 G. Devarajulu, O. Ravi, C. M. Reddy, S. Z. A. Ahamed and B. D. P. Raju, Spectroscopic properties and upconversion studies of $Er^{3+}$-doped $SiO_2$–$Al_2O_3$–$Na_2CO_3$–$SrF_2$–$CaF_2$ oxyfluoride glasses for optical amplifier applications, *J. Lumin.*, 2018, **194**, 499–506.

33 X. Y. Song, D. Y. Jin, D. C. Zhou, P. F. Xu and K. X. Han, $Er^{3+}/Yb^{3+}$ co-doped bismuthate glass and its large-mode-area double-cladding fiber for 1.53 μm laser, *J. Alloys Compd.*, 2021, **853**, 157305.

34 H. Desirena, E. D. L. Rosa, V. H. Romero, J. F. Castillo, L. A. Díaz-Torres and J. R. Oliva, Comparative study of the spectroscopic properties of $Yb^{3+}/Er^{3+}$ codoped tellurite glasses modified with $R_2O$ ($R$ = Li, Na and K), *J. Lumin.*, 2012, **132**, 391–397.

35 X. L. Zou and H. Toratani, Spectroscopic properties and energy transfers in $Tm^{3+}$ singly- and $Tm^{3+}/Ho^{3+}$ doubly-doped glasses, *J. Non-Cryst. Solids*, 1996, **195**, 113–124.

36 A. A. Reddy, S. S. Babu, K. Pradeesh, C. J. Otton and G. V. Prakash, Optical Properties of highly $Er^{3+}$-doped sodium-aluminium–phosphate glasses for broadband 1.5 μm emission, *J. Alloys Compd.*, 2011, **509**, 4047–4052.

37 I. Jlassi, H. Elhouichet, M. Ferid and C. Barthou, Judd-Ofelt analysis and improvement of thermal and optical properties of tellurite glasses by adding $P_2O_5$, *J. Lumin.*, 2010, **130**, 2394–2401.

38 M. Pokhrel, G. A. Kumar, S. Balaji, R. Debnath and D. K. Sardar, Optical characterization of $Er^{3+}$ and $Yb^{3+}$ co-doped barium fluorotellurite glass, *J. Lumin.*, 2012, **132**, 1910–1916.

39 K. Linganna, G. L. Agawane and J. H. Choi, Longer lifetime of $Er^{3+}/Yb^{3+}$ co-doped fluorophosphate glasses for optical amplifier applications, *J. Non-Cryst. Solids*, 2017, **471**, 65–71.

40 T. Wei, Y. Tian, F. Z. Chen, M. Z. Cai, J. J. Zhang, X. F. Jing, F. C. Wang, Q. Y. Zhang and S. Q. Xu, Mid-infrared fluorescence, energy transfer process and rate equation analysis in $Er^{3+}$ doped germanate glass, *Sci. Rep.*, 2014, **4**, 6060.